Acta Mechanica Solida Sinica, Vol. 28, No. 3, June, 2015 ISSN 0894-9166
Published by AMSS Press, Wuhan, China

AN INTEGRATED COUPLING ELEMENT FOR VEHICLE-RAIL-BRIDGE INTERACTION SYSTEM WITH A NON-UNIFORM CONTINUOUS BRIDGE**

Hongyin Yang[1] **Zhijun Chen**[1*] **Shaofan Li**[1,2] **Hailong Zhang**[1] **Jianping Fan**[1]

([1] *School of Civil Engineering and Mechanics, Huazhong University of Science and Technology, Wuhan* 430074, *China*)

([2] *Department of Civil and Environmental Engineering, University of California at Berkeley, Berkeley, CA* 94720, *USA*)

Received 25 June 2013, revision received 20 May 2014

ABSTRACT An integrated coupling element considering wheel-rail interface for analyzing the dynamic responses of vehicle-rail-bridge interaction system with a non-uniform continuous bridge is presented. The governing equations of the interaction system are established first, and the solution procedure and assembly method of the coupling element are demonstrated. Finally, the accuracy, efficiency and function of the integrated coupling element are tested using two numerical examples. The influences of different combinations of rail and bridge element length in the coupling element on the solution are investigated, and the effects of different rail irregularities on the dynamic responses are discussed.

KEY WORDS vehicle-rail-bridge dynamic interaction, integrated coupling element, non-uniform continuous beam, wheel-rail contact, rail irregularity

I. INTRODUCTION

High-speed railway transportation provides a viable alternative to both aviation and highway transportation; however, it continues to suffer new technical problems. Recently, the dynamic behaviors of bridges on high-speed railways have received increased attention, and many influential studies have been published over the past two decades[1–3]. In general, two types of methods, i.e., analytical and numerical methods, have been used in these investigations. Analytical methods are simple and clear, but not suitable for analyzing the complex dynamic behaviors of railway bridges[2]. However, the finite element method (FEM) has been widely used in this field as a powerful numerical means by many researchers[4–7]. Based on FEM and structural dynamics, various coupling elements have been proposed. Yang and Yau[4] first presented a vehicle-bridge element to model the vehicle-bridge dynamic interaction. Thereafter, Yang et al.[5] and Wu et al.[6] improved the vehicle-bridge element by considering the pitching effect of the vehicle. Ju and Lin[7] considered vehicle braking and acceleration in their analysis of a vehicle-bridge interaction system. In these studies, the vehicle-bridge element did not take into account the effects of rail structures, which were mainly applicable to the vehicle-bridge coupling system.

* Corresponding author. E-mail: chenzj@hust.edu.cn

** Project supported by the National Natural Science Foundation of China (No. 51078164).

However, maintenance workers of French and German railways have reported destabilization of the ballast on small and medium span bridges on high-speed railway lines[8]. This phenomenon could result in serious consequences, such as the possibility of derailment and increased maintenance costs. This means that rail structure cannot be ignored in the dynamic analysis of interaction system. Accordingly, Cheng et al.[9] developed a bridge-track-vehicle coupling element to examine the interactions of the train, the rail and the bridge. In order to provide an effective and convenient way to analyze train-track dynamics, Koh et al.[10] presented a new approach called the moving element method, which allowed the use of different element sizes for improving model efficiency. Based on the stationary value of the total potential energy of the coupling dynamic system, Lou[11] presented a vehicle-track-bridge interaction element considering the pitch effect of the vehicle to analyze the vehicle-track-bridge dynamic interaction, in which the vehicle was modelled as a two-axle mass-spring-damper system with 4 degrees of freedom (DOFs).

Considering the rail structure, Lou et al.[12,13] utilized the finite element method to analyze the vehicle-track-bridge interaction by modelling the vehicle as a mass-spring-damper system with 10 DOFs. Lou et al.[14] also developed a special rail-bridge coupling element to improve the computational efficiency, in which the length of the uniform bridge element was longer than that of the rail element. In the two methods, the rail and the bridge were modelled as an elastic Bernoulli-Euler upper beam and a simply supported Bernoulli-Euler lower beam, respectively, while the elasticity and damping properties of the ballast were represented by continuous springs and dampers, respectively. It is true the aforementioned analytic models can be used in vehicle-track-bridge systems, they simplify the interaction between the wheel and the rail. Since the wheelsets are assumed to always maintain contact with the rail, these approaches cannot simulate the jump of wheels or derailment.

As transient jump of wheel can occur, the wheel-rail contact should be simulated more precisely. Contact models using linear or nonlinear Hertz springs have been widely used to examine the interaction between the wheel and the rail, with many notable achievements reported in the past decade or so[15–19]. Cheng et al.[20] investigated the onset and effects of separation between a moving vehicle and the bridge. Using a linear Hertz spring to model the wheel-rail contact, Bowe and Mullarkey[21] and Zhang et al.[22] analyzed the dynamic responses of the train-bridge interaction. Besides, adopting the same contact model, Liu et al.[23] studied the separation between a vehicle and the bridge, and by considering random and abrupt irregularity on the bridge, the transient jump of wheel was also discussed. It is worthwhile to point out that these analytic models are almost all oriented toward structures with girders of uniform cross-section and depth.

Although the non-uniform geometric properties of bridges make the vehicle-rail-bridge system complicated, it has still received considerable attention from researchers owing to the demands of practical engineering. Leung[24] presented a new method to form the element matrices for non-uniform frames based on the Galerkin method. Zheng et al.[25] analyzed the vibration of a multi-span non-uniform beam under moving loads using the modified beam vibration functions. Using both the modal analysis method and the direct integration method, Dugush and Eisenberger[26] investigated the dynamic behavior of multi-span non-uniform beams travelled over by a moving load. Furthermore, by modelling the structure as Bernoulli-Euler beam elements, Martínez-Castro et al.[27] presented a semi-analytic solution for the moving load problem, which is of great importance to the analysis of multi-span non-uniform beams subjected to moving forces, such as high-speed trains. Based on practical engineering applications for high-speed railway bridges, a comprehensive model of the vehicle-rail-bridge interaction system should address not only the vibration of the vehicle, the rail and the bridge, but also the wheel-rail contact and the rail-bridge connection. Unfortunately, few of the research objectives were addressed in existing studies (at most 1 or 2 of them) to merit mention. Thus, in order to meet the requirements of complex railway bridges, it is necessary to develop a powerful integrated coupling element for the vehicle-rail-bridge interaction.

In this paper, an integrated coupling element for analyzing the dynamic responses of a multi-span non-uniform continuous bridge travelled over by high-speed trains is presented. In this vehicle-rail-bridge interaction model, the vehicle is modelled as a mass-spring-damper system with 10 DOFs, with the rail bed represented by continuous springs and dampers. Wheel-rail contact interaction is simulated by a series of linear Hertz springs[21–23], while the rail and the bridge are modelled as an elastic Bernoulli-Euler upper beam with finite length and a multi-span non-uniform Bernoulli-Euler

lower beam, respectively. A simplified calculation method is introduced for the non-uniform continuous bridge. Based on the substructure principle[28], the vehicle, the rail and the bridge are seen as three interactive subsystems. The motion equations of the three subsystems are first established separately, and the coupling element can be easily assembled in correspondence with different analytical purposes and design requirements. Then, the solution procedure of the problem is demonstrated, and the flow chart of assembly and calculation is given. The computational program is coded in MATLAB, by which the dynamic responses of each subsystem can be obtained simultaneously. Finally, the accuracy, efficiency and function of the integrated coupling element and the program are tested using two numerical examples. The influences of different combinations of rail and bridge element length are investigated, and the effects of rail random and abrupt irregularities on the dynamic responses are also discussed.

II. EQUATIONS OF MOTION FOR THE TRAIN-RAIL-BRIDGE INTERACTION SYSTEM

Figure 1 shows the vertical model of a train moving on a multi-span non-uniform continuous bridge, in which the rail, the vehicles, the bridge and the embankments are modelled. The bridge is modelled as a linear elastic continuous Bernoulli-Euler beam resting on simple supports at the top of piers, and the rail is simulated by a linear elastic Bernoulli-Euler beam with both ends clamped. With the wheel-rail contact modelled by a Hertz spring, the finite element model of the vehicle system and the rail-bridge system are shown in Fig.2. The elasticity and damping properties of the rail bed are represented by continuous springs and dampers characterized by k_{rr}, k_{rb}, c_{rr} and c_{rb}, respectively. Figure 3 shows a vehicle-rail interaction system with the ith vehicle. A detailed description of the model parameters can be found in Ref.[13].

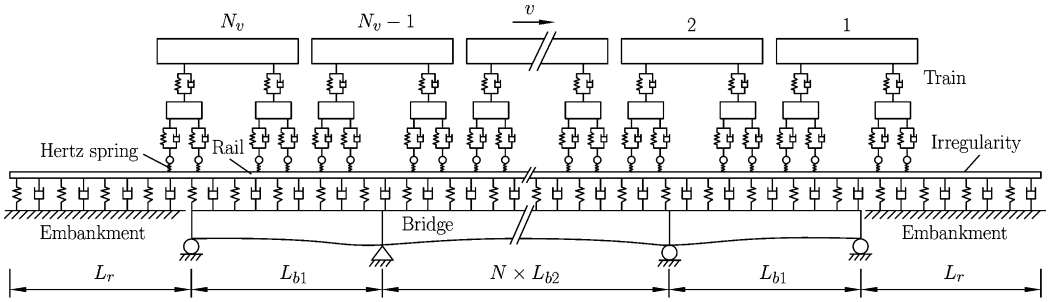

Fig. 1. Model of a multi-span non-uniform continuous bridge traveled by a high-speed train.

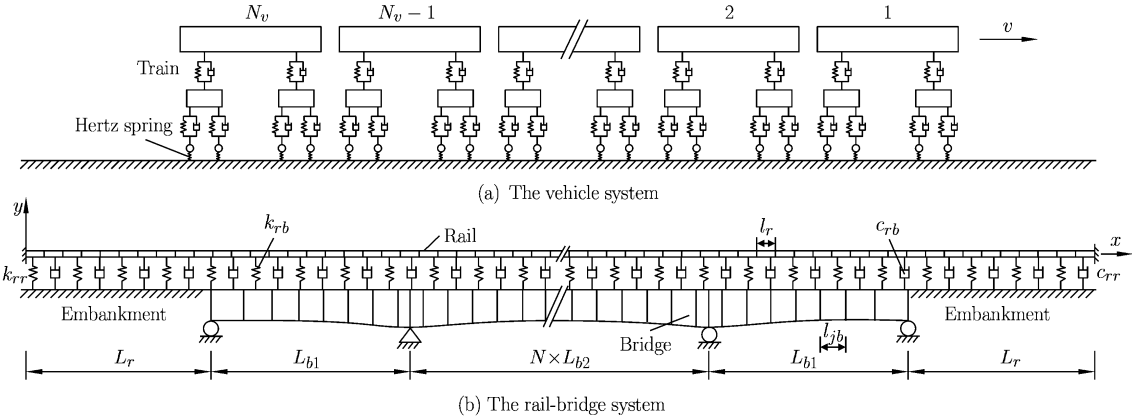

Fig. 2. Finite element model.

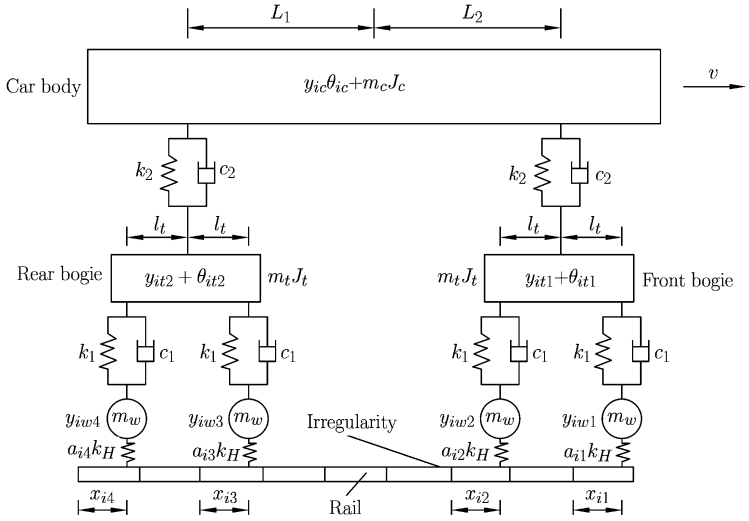

Fig. 3. A vehicle-rail interaction system with the ith vehicle.

It is assumed that if certain vehicles are not on the rail in question, they are supported on a rigid foundation. Let $r(x)$ denote the initial irregularities of the rail.

2.1. Wheel-Rail Contact Model

The interaction between the wheel and the rail represents not only the connection of the vehicle and the lower structures, but also the main excitation source of the two vibration subsystems. There are two widely used models in dealing with the wheel-rail contact[16]. One is to assume the wheel-rail relationship with rigid contact, with no elastic deformation considered[11–14]. Although the calculation with this method is simple, it cannot simulate wheel jumps. The other is considering the wheel-rail interface and the elastic deformation[21–23]. Since jumps of wheels can occur[23], the second wheel-rail contact model is more accurate for the actual response. According to Fig.3, a Hertz spring with stiffness k_H that cannot be extended is introduced to simulate the wheel-rail contact. In the mathematical model, the spring coefficient is $a_{in}k_H$, and a_{in} has the following properties[2,3,23]:

$$a_{in}=\begin{cases}1, \text{ spring be condensed}\\ 0, \text{ spring be extended}\end{cases} \tag{1}$$

where a_{in} $(i=1,2,\ldots,N_v;\ n=1,2,3,4)$ denotes the wheel-rail contact coefficient of the nth wheel of the ith vehicle. When the wheelset is on a rigid foundation, $a_{in}=1$.

The spring deformation can be written as

$$y_{in}=y_{iwn}-y_{irn}-r(x_{in}) \tag{2}$$

where y_{in} $(i=1,2,\ldots,N_v;\ n=1,2,3,4)$ is the deformation of the nth wheel of the ith vehicle; x_{in} is the local coordinate; y_{iwn} is the vertical wheel displacement; y_{irn} is the vertical rail displacement at x_{in}; $r(x_{in})$ denotes the rail irregularity at x_{in}.

The contact force F_{in} $(i=1,2,\ldots,N_v;\ n=1,2,3,4)$ can be written as

$$F_{in}=-a_{in}k_Hy_{in} \tag{3}$$

2.2. Equations of Motion for the Bridge

Figure 4 shows a typical rail-bridge coupling element with unequal element lengths, in which the rail is divided into a number of beam elements with equal length l_r and the bridge is divided into a series of non-uniform beam elements with length l_{jb} $(l_{jb}>l_r)$. The motion of the jth bridge element is controlled by the following second-order equation:

$$\left[M_{jb}^e\right]\left\{\ddot{q}_{jb}^e\right\}+\left[C_{jb}^e\right]\left\{\dot{q}_{jb}^e\right\}+\left[K_{jb}^e\right]\left\{q_{jb}^e\right\}=\left\{P_{jb}^e\right\}-\int_0^{l_{jb}}[N]_{jb}^{\mathrm{T}}f_{jrb}(x_j,t)\mathrm{d}x \tag{4}$$

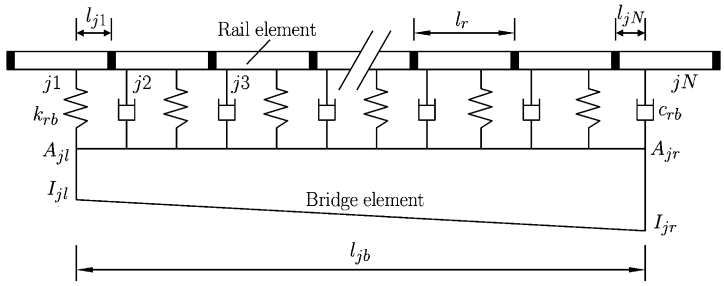

Fig. 4. Typical rail-bridge coupling element with unequal lengths.

where $\left[M^e_{jb}\right] = \int_0^{l_{jb}} \rho_b A_{jb}(x_j)[N]^{\mathrm{T}}_{jb}[N]_{jb}\mathrm{d}x$, $\left[K^e_{jb}\right] = \int_0^{l_{jb}} E_b I_{jb}(x_j)[N'']^{\mathrm{T}}_{jb}[N'']_{jb}\mathrm{d}x$ and $\left[C^e_{jb}\right]$ denote the element mass, stiffness and damping matrices, respectively; $\left\{\ddot{q}^e_{jb}\right\}$, $\left\{\dot{q}^e_{jb}\right\}$, $\left\{q^e_{jb}\right\}$ and $\left\{P^e_{jb}\right\}$ denote the nodal acceleration, velocity, displacement and external load vectors, respectively; ρ_b, $A_{jb}(x_j)$, E_b, $I_{jb}(x_j)$ and x_j are the bridge mass density, cross-sectional area, modulus of elasticity, moment of inertia and local coordinate, respectively. $f_{jrb}(x_j, t)$ is the distributed load from the rail, given by

$$f_{jrb}(x_j, t) = -k_{rb}(y_{mr} - y_{jb}) - c_{rb}(\dot{y}_{mr} - \dot{y}_{jb}) \tag{5}$$

$[N]_{jb}$ represents the cubic Hermitian FEM shape functions, given by

$$[N]_{jb} = \left[N_1\ N_2\ N_3\ N_4\right]_{x=x_j, l=l_{jb}} \tag{6}$$

where $N_1 = 1 - 3\left(\frac{x}{l}\right)^2 + 2\left(\frac{x}{l}\right)^3$, $N_2 = x\left(1 - \frac{x}{l}\right)^2$, $N_3 = 3\left(\frac{x}{l}\right)^2 - 2\left(\frac{x}{l}\right)^3$, $N_4 = x\left[\left(\frac{x}{l}\right)^2 - \frac{x}{l}\right]$.

Bridge displacement y_{jb} can be expressed in terms of the shape functions and nodal displacements of the bridge element:

$$y_{jb} = [N]_{jb}\left\{q^e_{jb}\right\} \tag{7}$$

and the time differentiation of y_{jb} can be written as

$$\dot{y}_{jb} = [N]_{jb}\left\{\dot{q}^e_{jb}\right\} \tag{8}$$

Substituting Eqs.(5)-(8) into Eq.(4), one obtains

$$\left[M^e_{jb}\right]\left\{\ddot{q}^e_{jb}\right\} + \left(\left[C^e_{jb}\right] + \left[C^e_{jbe}\right]\right)\left\{\dot{q}^e_{jb}\right\} + \left(\left[K^e_{jb}\right] + \left[K^e_{jbe}\right]\right)\left\{q^e_{jb}\right\} = \left\{P^e_{jbe}\right\} \tag{9}$$

where $\left\{P^e_{jbe}\right\} = \sum_{m=1}^{m=N}\int_0^{l_{jb}} [N]^{\mathrm{T}}_{jb}k_{rb}y^e_{mr}\mathrm{d}x + \sum_{m=1}^{m=N}\int_0^{l_{jb}} [N]^{\mathrm{T}}_{jb}c_{rb}\dot{y}^e_{mr}\mathrm{d}x$ is the equivalent node load vector; $\left[K^e_{jbe}\right] = \int_0^{l_{jb}} k_{rb}[N]^{\mathrm{T}}_{jb}\,[N]_{jb}\,\mathrm{d}x$ and $\left[C^e_{jbe}\right] = \int_0^{l_{jb}} c_{rb}[N]^{\mathrm{T}}_{jb}\,[N]_{jb}\,\mathrm{d}x$ are the additional stiffness and damping matrices, respectively; the subscript m denotes the rail element number.

Here, it is interesting to note that all the additional matrices and the equivalent node load vector in Eq.(9) are only caused by stiffness k_{rb} and damping coefficient c_{rb} of the rail bed. Similarly, the rail displacement $y_{mr}(m = 1, 2, \ldots, N)$ and its differentiation can be written as

$$y_{mr} = [N]_{mr}\left\{q^e_{mr}\right\} \tag{10}$$

$$\dot{y}_{mr} = [N]_{mr}\left\{\dot{q}^e_{mr}\right\} \tag{11}$$

where $[N]_{mr} = \left[N_1\ N_2\ N_3\ N_4\right]_{x=x_m, l=l_r}$, and x_m is the local coordinate of the rail element.

Substituting Eqs.(10)-(11) into Eq.(9), one obtains

$$\begin{aligned}&\left[M^e_{jb}\right]\left\{\ddot{q}^e_{jb}\right\} + \left(\left[C^e_{jb}\right] + \left[C^e_{jbe}\right]\right)\left\{\dot{q}^e_{jb}\right\} + \left(\left[K^e_{jb}\right] + \left[K^e_{jbe}\right]\right)\left\{q^e_{jb}\right\}\\ &\quad - \sum_{m=1}^{m=N}\left[C^e_{mrb}\right]\left\{\dot{q}^e_{mr}\right\} - \sum_{m=1}^{m=N}\left[K^e_{mrb}\right]\left\{q^e_{mr}\right\} = 0\end{aligned} \tag{12}$$

where

$$[C^e_{mrb}]=\begin{cases}\displaystyle\int_0^{l_{j1}} c_{rb}[N]^{\mathrm{T}}_{jb}[N]_{1r}\mathrm{d}x & (m=1)\\ \displaystyle\int_{l_{j1}+(m-1)l_r}^{l_{j1}+(m-2)l_r} c_{rb}[N]^{\mathrm{T}}_{jb}[N]_{mr}\mathrm{d}x & (m=2,3,\cdots,N-1)\\ \displaystyle\int_{l_{j1}+(N-2)l_r}^{l_{jb}} c_{rb}[N]^{\mathrm{T}}_{jb}[N]_{Nr}\mathrm{d}x & (m=N)\end{cases} \tag{13}$$

The matrix $[K^e_{mrb}]$ can be obtained by simply replacing c in the corresponding damping matrix $[C^e_{mrb}]$ with k, and the local coordinate transformation should be adopted for x_m to make its coordinate consistent with x_j.

Let $l_{j1}=l_{jN}=l_r$, $N=1$, and Eq.(12) becomes the equation of motion of the bridge for the case rail-bridge coupling element with equal lengths.

According to Fig.4, the expressions of the element mass and stiffness matrices in Eq.(4), i.e., $\left[M^e_{jb}\right]$ and $\left[K^e_{jb}\right]$, respectively, are very complex for non-uniform bridge elements. In order to simplify the calculation of the two matrices of the complex non-uniform beam element, the variations of cross-sectional area $A_{jb}(x_j)$ and moment of inertia $I_{jb}(x_j)$ can be assumed to be linear for all non-uniform elements. So $A_{jb}(x_j)$ can be expressed as follows:

$$A_{jb}(x_j)=A_{jl}+\frac{A_{jr}-A_{jl}}{l_{jb}}x_j \tag{14}$$

where A_{jl} and A_{jr} denote the cross-sectional area of the jth element at the left node and right node, respectively. The function $I_{jb}(x_j)$ can be obtained by simply replacing A in the corresponding function $A_{jb}(x_j)$ with I.

Conventionally, structural damping is computed at the structural level. Based on the definition of Rayleigh damping, element damping matrix $\left[C^e_{jb}\right]$ of the bridge in Eq.(4) is computed as follows:

$$\left[C^e_{jb}\right]=\alpha_0\left[M^e_{jb}\right]+\alpha_1\left[K^e_{jb}\right] \tag{15}$$

where, given the damping ratio ζ, the two coefficients α_0 and α_1 can be determined as

$$\alpha_0=\frac{2\zeta\omega_1\omega_2}{\omega_1+\omega_2},\quad \alpha_1=\frac{2\zeta}{\omega_1+\omega_2} \tag{16}$$

Here, ω_1 and ω_2 are the first and second frequencies of vibration, respectively, of the railway bridge.

2.3. Equations of Motion for the Rail

As shown in Fig.2(b), the motion of the mth rail element is controlled by the following second-order equation:

$$[M^e_{mr}]\{\ddot{q}^e_{mr}\}+[C^e_{mr}]\{\dot{q}^e_{mr}\}+[K^e_{mr}]\{q^e_{mr}\}=\{P^e_{mr}\}-\int_0^{l_r}[N]^{\mathrm{T}}_{mr}f_{mbr}(x_m,t)\mathrm{d}x-\sum[N]^{\mathrm{T}}_{nr}F_{in} \tag{17}$$

where $[M^e_{mr}]=\displaystyle\int_0^{l_r}\rho_r A_r[N]^{\mathrm{T}}_{mr}[N]_{mr}\mathrm{d}x$, $[K^e_{mr}]=\displaystyle\int_0^{l_r}E_r I_r[N'']^{\mathrm{T}}_{mr}[N'']_{mr}\mathrm{d}x$ and $[C^e_{mr}]$ denote the element mass, stiffness and damping matrices, respectively; $\{\ddot{q}^e_{mr}\}$, $\{\dot{q}^e_{mr}\}$, $\{q^e_{mr}\}$ and $\{P^e_{mr}\}$ denote the nodal acceleration, velocity, displacement and external load vectors, respectively; ρ_r, A_r, E_r, I_r and x_m are the rail mass density, cross-sectional area, modulus of elasticity, moment of inertia and local coordinate, respectively; $f_{mbr}(x_m,t)$ is the distributed load from the embankment or the bridge; F_{in} is the concentrated load from the nth wheel of the ith vehicle; $[N]_{nr}=\left[N_1\ N_2\ N_3\ N_4\right]_{x=x_{in},l=l_r}$; x_{in}(n=1, 2, 3, 4) denotes the distance between the left end of the rail element, on which the nth wheel of the ith vehicle is located, and the location of the nth wheel of the ith vehicle.

Based on the linear elastic theory, the dynamic response caused by each load in Eq.(17) can be calculated first, and then the total dynamic response can be obtained by using the superposition

principle. When there is no wheelset located on the mth rail element supported on the embankment, the equation of motion can be written as follows:

$$[M^e_{mr}]\{\ddot{q}^e_{mr}\} + [C^e_{mr}]\{\dot{q}^e_{mr}\} + [K^e_{mr}]\{q^e_{mr}\} = -\int_0^{l_r} [N]^{\mathrm{T}}_{mr} f_{mbr}(x_m, t)\mathrm{d}x \tag{18}$$

where

$$f_{mbr}(x_m, t) = k_{rr}y_{mr} + c_{rr}\dot{y}_{mr} = k_{rr}[N]_{mr}\{q^e_{mr}\} + c_{rr}[N]_{mr}\{\dot{q}^e_{mr}\} \tag{19}$$

Substituting Eq.(19) into Eq.(18), one obtains

$$[M^e_{mr}]\{\ddot{q}^e_{mr}\} + ([C^e_{mr}] + [C^e_{mre}])\{\dot{q}^e_{mr}\} + ([K^e_{mr}] + [K^e_{mre}])\{q^e_{mr}\} = 0 \tag{20}$$

where $[C^e_{mre}] = \int_0^{l_r} c_{rr}[N]^{\mathrm{T}}_{mr}[N]_{mr}\,\mathrm{d}x$ and $[K^e_{mre}] = \int_0^{l_r} k_{rr}[N]^{\mathrm{T}}_{mr}[N]_{mr}\,\mathrm{d}x$ are the additional damping matrix and the additional stiffness matrix, respectively.

When there is no wheelset located on the mth rail element supported on the bridge, the equation of motion can be also written as Eq.(18), where

$$f_{mbr}(x_m, t) = k_{rb}(y_{mr} - y_{jb}) + c_{rb}(\dot{y}_{mr} - \dot{y}_{jb}) \tag{21}$$

Substituting Eq.(21) into Eq.(18), one further obtains

$$\begin{aligned}[M^e_{mr}]\{\ddot{q}^e_{mr}\} + ([C^e_{mr}] + [C^e_{mrbe}])\{\dot{q}^e_{mr}\} + ([K^e_{mr}] + [K^e_{mrbe}])\{q^e_{mr}\} \\ - \sum [C_{jbr}]\{\dot{q}^e_{jb}\} - \sum [K_{jbr}]\{q^e_{jb}\} = 0\end{aligned} \tag{22}$$

where $[C^e_{mrbe}] = \int_0^{l_r} c_{rb}[N]^{\mathrm{T}}_{mr}[N]_{mr}\,\mathrm{d}x$ and $[K^e_{mrbe}] = \int_0^{l_r} k_{rb}[N]^{\mathrm{T}}_{mr}[N]_{mr}\,\mathrm{d}x$ are the additional damping matrix and the additional stiffness matrix, respectively.

According to the symmetry of system matrices, the last two terms on the left side of Eq.(22) can be obtained from those of Eq.(12).

When there is one wheelset located on the mth rail element, the equation of motion can be written as

$$[M^e_{mr}]\{\ddot{q}^e_{mr}\} + [C^e_{mr}]\{\dot{q}^e_{mr}\} + [K^e_{mr}]\{q^e_{mr}\} = -[N]^{\mathrm{T}}_{nr}F_{in} \tag{23}$$

Substituting Eq.(3) into Eq.(23), one obtains

$$[M^e_{mr}]\{\ddot{q}^e_{mr}\} + [C^e_{mr}]\{\dot{q}^e_{mr}\} + ([K^e_{mr}] + [K^e_{mrw}])\{q^e_{mr}\} - a_{in}k_H[N]^{\mathrm{T}}_{mr,x=x_{in}}y_{iwn} = \{P^e_{mrw}\} \tag{24}$$

where $[K^e_{mrw}] = a_{in}k_H[N]^{\mathrm{T}}_{mr,x=x_{in}}[N]_{mr,x=x_{in}}$ and $\{P^e_{mrw}\} = -a_{in}k_H r(x_{in})[N]^{\mathrm{T}}_{mr,x=x_{in}}$ are the additional stiffness matrix and the equivalent node load vector, respectively.

If more than one wheelset are located on the mth rail element, Eq.(24) is also suitable for the other wheelsets.

2.4. Equations of Motion for the Train

The classical vehicle model with 10 DOFs is shown in Fig.3, and the equations of motion can be written as[23]

$$[M_{iv}]\{\ddot{q}_{iv}\} + [C_{iv}]\{\dot{q}_{iv}\} + [K_{iv}]\{q_{iv}\} = \{P_{iv}\} \tag{25}$$

where the subscript i denotes the ith vehicle.

Vehicle displacement vector $\{q_{iv}\}$ can be written as

$$\{q_{iv}\} = \left\{ y_{iw1}\ y_{iw2}\ y_{iw3}\ y_{iw4}\ y_{it1}\ \theta_{it1}\ y_{it2}\ \theta_{it2}\ y_{ic}\ \theta_{ic} \right\}^{\mathrm{T}} \tag{26}$$

Vehicle mass matrix $[M_{iv}]$ can be written as

$$[M_{iv}] = \mathrm{diag}\left[m_w\ m_w\ m_w\ m_w\ m_t\ J_t\ m_t\ J_t\ m_c\ J_c \right] \tag{27}$$

Vehicle stiffness matrix $[K_{iv}]$ can be written as

$$[K_{iv}]=\begin{bmatrix} k_1 & 0 & 0 & 0 & -k_1 & -l_tk_1 & 0 & 0 & 0 & 0 \\ 0 & k_1 & 0 & 0 & -k_1 & l_tk_1 & 0 & 0 & 0 & 0 \\ 0 & 0 & k_1 & 0 & 0 & 0 & -k_1 & -l_tk_1 & 0 & 0 \\ 0 & 0 & 0 & k_1 & 0 & 0 & -k_1 & l_tk_1 & 0 & 0 \\ -k_1 & -k_1 & 0 & 0 & 2k_1+k_2 & 0 & 0 & 0 & -k_2 & -k_2L_2 \\ -l_tk_1 & l_tk_1 & 0 & 0 & 0 & 2l_t^2k_1 & 0 & 0 & 0 & 0 \\ 0 & 0 & -k_1 & -k_1 & 0 & 0 & 2k_1+k_2 & 0 & -k_2 & k_2L_1 \\ 0 & 0 & -l_tk_1 & l_tk_1 & 0 & 0 & 0 & 2l_t^2k_1 & 0 & 0 \\ 0 & 0 & 0 & 0 & -k_2 & 0 & -k_2 & 0 & 2k_2 & k_2(L_2-L_1) \\ 0 & 0 & 0 & 0 & -k_2L_2 & 0 & k_2L_1 & 0 & k_2(L_2-L_1) & k_2(L_1^2+L_2^2) \end{bmatrix} \tag{28}$$

where L_1, L_2 and l_t denote the horizontal distance between the center of gravity of the car body and the rear bogie, the horizontal distance between the center of gravity of the car body and the front bogie and half of the bogie axle base, respectively.

Vehicle damping matrix $[C_{iv}]$ can be obtained by simply replacing k in the corresponding stiffness matrix $[K_{iv}]$ with c.

Vehicle load vector $\{P_{iv}\}$ can be written as

$$\{P_{iv}\}=\left\{\, m_wg+F_{i1}\ \ m_wg+F_{i2}\ \ m_wg+F_{i3}\ \ m_wg+F_{i4}\ \ m_tg\ \ 0\ \ m_tg\ \ 0\ \ m_cg\ \ 0 \,\right\}^{\mathrm{T}} \tag{29}$$

Here, it should be noted that the load of the wheel consists of the gravity and the contact force, and the motion equation for the wheelset caused by the contact force can be written as

$$m_w\ddot{y}_{iwn}+c_1\dot{y}_{iwn}+k_1y_{iwn}+P_{itn}=F_{in}\quad(n=1,2,3,4) \tag{30}$$

where P_{itn} is the total force caused by the DOFs of the car body and the bogie.

If the wheelset is supported on the rail, substituting Eq.(3) into Eq.(30), one obtains

$$m_w\ddot{y}_{iwn}+c_1\dot{y}_{iwn}+(k_1+a_{in}k_H)y_{iwn}-a_{in}k_H[N]_{mr,x=x_{in}}\{q^e_{mr}\}+P_{itn}=a_{in}k_Hr(x_{in}) \tag{31}$$

If the wheelset is supported on a rigid foundation, one can obtain

$$m_w\ddot{y}_{iwn}+c_1\dot{y}_{iwn}+(k_1+a_{in}k_H)y_{iwn}+P_{itn}=0 \tag{32}$$

III. SOLUTION PROCEDURES

The equations of motion can be written in sub-matrix form for the vehicle-rail-bridge interaction system shown in Fig.1 as follows:

$$\begin{bmatrix} M_{bb} & 0 & 0 \\ 0 & M_{rr} & 0 \\ 0 & 0 & M_{vv} \end{bmatrix}\begin{Bmatrix} \ddot{q}_b \\ \ddot{q}_r \\ \ddot{q}_v \end{Bmatrix}+\begin{bmatrix} C_{bb} & C_{rb} & 0 \\ C_{br} & C_{rr} & 0 \\ 0 & 0 & C_{vv} \end{bmatrix}\begin{Bmatrix} \dot{q}_b \\ \dot{q}_r \\ \dot{q}_v \end{Bmatrix}+\begin{bmatrix} K_{bb} & K_{rb} & 0 \\ K_{br} & K_{rr}+K_{cr} & K_{cvr} \\ 0 & K_{crv} & K_{vv} \end{bmatrix}\begin{Bmatrix} q_b \\ q_r \\ q_v \end{Bmatrix}=\begin{Bmatrix} F_b \\ F_r+F_{cr} \\ F_v+F_{cv} \end{Bmatrix} \tag{33}$$

where M, C and K denote the mass, damping and stiffness sub-matrices, respectively; q and F denote the displacement and force sub-vectors, respectively; subscripts b, r, v and c denote the bridge, rail, vehicle and interaction effects, respectively.

Figure 5 shows the flow chart of assembly and calculation. Based on the equations in §II, the assembly of the matrix equation of the dynamic system (Eq.(33)) is further explained as follows:

1. Assemble the equations of motion for the rail-bridge system shown in Fig.2(b) to avoid any vehicle actions according to Eqs.(12), (20) and (22), and form sub-matrices M_{bb}, M_{rr}, C_{bb}, C_{rr}, C_{rb}, C_{br}, K_{bb}, K_{br}, K_{rr} and K_{rb} as well as sub-vectors F_b and F_r.

2. Assemble the equations of motion for the vehicle system supported on a rigid foundation shown in Fig.2(a) according to Eqs.(25) and (32), and form sub-matrices M_{vv}, C_{vv} and K_{vv} as well as sub-vector F_v.

3. Take the above equations obtained as the initial equations of motion for each time step; form sub-matrices K_{cr}, K_{cvr} and K_{crv} and sub-vectors F_{cr} and F_{cv} caused by the wheel-rail contact according to Eqs.(24) and (31) at each time step, and then add them to the initial equations of motion.

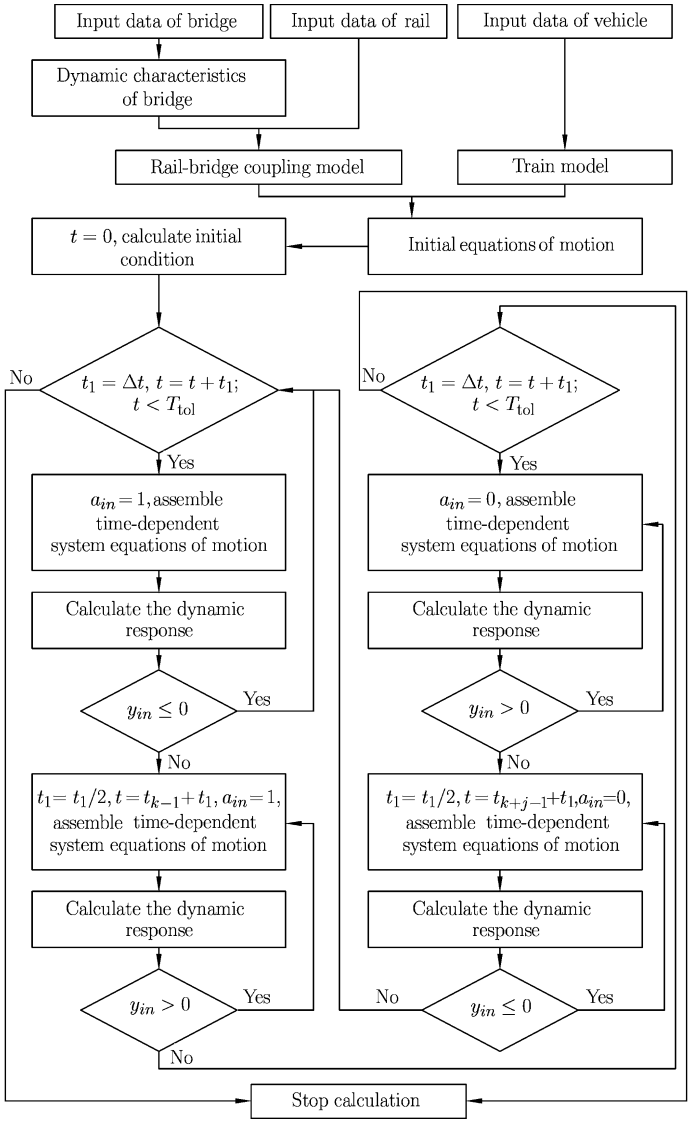

Fig. 5. Flow chart of assembly and calculation.

It should be noted that only sub-matrices K_{cr}, K_{cvr} and K_{crv} and sub-vectors F_{cr} and F_{cv} are time-dependent, and they must be calculated at each time step.

As shown in Fig.5, the variable step algorithm is adopted to determine the occurrence time of the transient jump of the wheel, which is very important for the accuracy of the solution. The main solution steps are summarized as follows:

1. Let Δt be the time step, $a_{in} = 1$ for the next step; calculate the system responses by direct time integration. If distance $y_{in} \le 0$ for the kth integration step, and the kth time is less than the total time, i.e., $t_k < T_{\text{tol}}$, continue. Otherwise, go back to the $(k-1)$th integration step.

2. Let the time step be half of the last calculation; recalculate the dynamic response of the kth integration step. If distance $y_{in} > 0$, go to step 2. Otherwise, go to step 3.

3. Let Δt be the time step, $a_{in} = 0$ for the next step; if distance $y_{in} > 0$ for the $(k+j)$th step and $t_{k+j} < T_{\text{tol}}$, continue. Otherwise, go back to the $(k+j-1)$th integration step.

4. Let the time step be half of the last calculation; recalculate the dynamic response of the $(k+j)$th integration step. If distance $y_{in} \le 0$, go to step 4. Otherwise, go to step 1.

IV. NUMERICAL EXAMPLES

In this section, two numerical examples are presented to demonstrate the capability and reliability of the coupling element proposed in this paper. Without iteration, the Newmark-β method with $\beta = 0.25$ and $\gamma = 0.5$ is adopted to solve the equations of motion for the vehicle-rail-bridge interaction system[5], and the time step Δt is 0.001 s.

4.1. A Three-span Continuous Haunched Beam Travelled over by a Moving Mass

Figure 6 shows a three-span haunched beam under a moving mass with a mass of $m = 1000$ kg. The beam parameters are the same as Ref.[27]. The travelling speed is 100 m/s, and the Hertz spring stiffness k_H is 5×10^9 N/m.

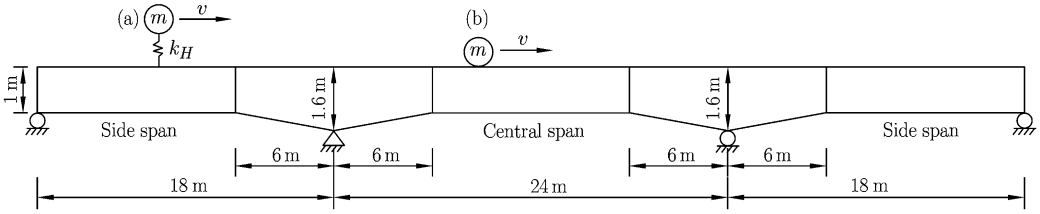

Fig. 6. A mass passes a non-uniform beam: (a) Present model; (b) Traditional moving-mass model.

Table 1. **Natural frequencies of the haunched beam (Hz)**

Mode	Dugush et al.[26]	Martínez-Castro et al.[27]	Present method
1	3.9198	3.9200	3.9258
2	6.6589	6.6592	6.6721
3	9.2381	9.2386	9.2624
4	15.8281	15.8294	15.8728
5	22.9430	22.9459	23.0090

The beam is divided into 30 equal elements, each with a length of 2 m. Based on the simplified calculation method developed for the complex non-uniform beam in §2.2, the first five natural frequencies are listed in Table 1, where the results of Martínez-Castro et al.[27] and Dugush et al.[26] are also listed. It can be seen that the results of different methods show good agreement, indicating that the simplified method can guarantee great accuracy.

Without irregularity, a moving spring mass model[22,23] with the present contact model shown in Fig.6(a) , which is different from the traditional moving-mass model[2,4] shown in Fig.6(b), is used to study the interaction between vehicle and bridge. The mid-span vertical displacement and acceleration of the central span are shown in Figs.7 and 8, respectively. Figure 9 shows the time history of the contact force between the mass and the beam. It is clear that the results of the two different models agree quite well with each other. This indicates that the present model with an appropriate contact stiffness, which is almost rigid, can yield a consistent result with the traditional moving-mass model.

The influence of irregularity on the dynamic response and the jump of mass can be calculated by the present model. Figure 10 shows the time history of the contact force considering irregularity, in sine function form $r(x) = 0.008 \sin(\pi x/24)$ m at the central span. The results of the two models are very consistent before the occurrence of the jump, i.e., $t < 0.196$ s. In the following time, however, many incorrect tensions can be clearly observed in the traditional moving-mass model, because it ignores the jumps of mass. But the contact force of the present model equals zero at certain times, indicating the jumps of mass. Besides, because of the jumps of mass, the phase and frequency of the responses between the two models are significantly different.

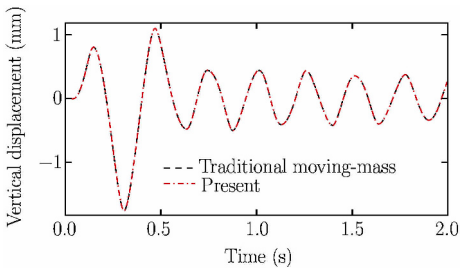

Fig. 7. Mid-span vertical displacement of the central span.

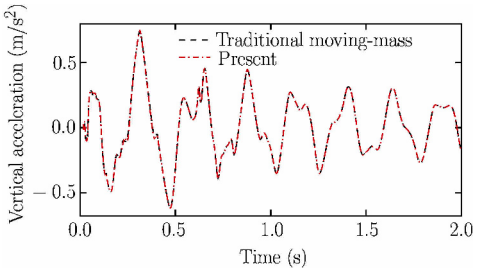

Fig. 8. Mid-span vertical acceleration of the central span.

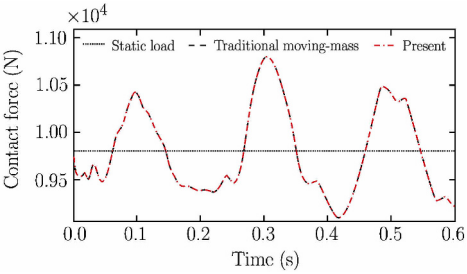

Fig. 9. Contact force between the mass and the beam.

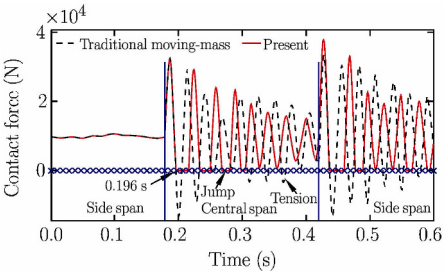

Fig. 10. Contact force between the mass and the beam with irregularity.

4.2. A Four-span Non-uniform Continuous Box Girder Railway Bridge Traveled on by a Train Consisting of Five Identical Vehicles

As shown in Fig.11(a), the length of each side span is 32 m, and the length of each central span is 48 m. With the balanced cantilever method[29], the bridge is divided into 42 segments during the segmental construction stages, and the segment lengths are arranged as: 1 m + 4×4 m + 5 m + 2×4 m + 2 m for the two side spans and 2 m + 2×4 m + 5 m + 4 m + 2×5 m + 4 m + 5 m + 2×4 m + 2 m for the two central spans. A parabolic variation of the depth with a length of 17 m exists in the sections close to the intermediate supports. As shown in Fig.11(b), the non-uniform section is divided into 17 equal elements, each with a length of 1 m, so there are 18 key sections of the bridge in total. The cross-section is shown in Fig.11(c). The parameters of the key sections calculated by ANSYS are listed in Table 2.

The following parameters are used for the vehicle and the rail[12]: $m_c = 4.175\times10^4$ kg; $J_c = 2.08\times10^6$ kg·m^2; $m_t = 3.04\times10^3$ kg; $J_t = 3.93\times10^3$ kg·m^2; $m_w = 1.78\times10^3$ kg; $k_2 = 5.3\times10^5$ N/m; $k_1 = 1.18\times10^6$ N/m; $c_2 = 9.02\times10^4$ N·s/m; $c_1 = 3.92\times10^4$ N·s/m; $L_1 = L_2 = 8.75$ m; and $l_t = 1.25$ m. The total longitudinal length of the rail structure is 220 m (it is assumed that the length of the rail on each approach

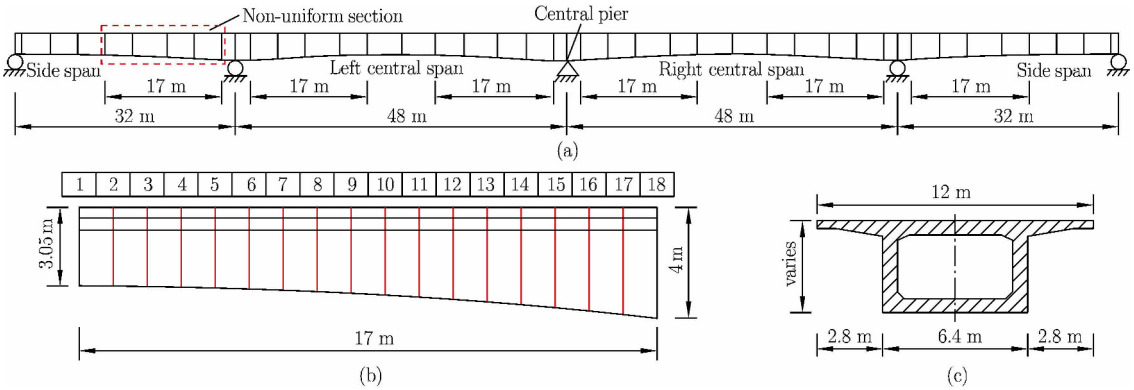

Fig. 11. Bridge model: (a) Elevation of the bridge with 42 segments; (b) Numbering of a key section of the non-uniform section; (c) Cross-section.

Table 2. **Parameters of the key sections of bridge**

Section	1	2	3	4	5	6	7	8	9
A_b (m^2)	8.8695	8.8819	8.9192	8.9816	9.0694	9.183	9.323	9.4899	9.6847
I_b (m^4)	12.229	12.275	12.412	12.643	12.969	13.396	13.927	14.568	15.328
Section	10	11	12	13	14	15	16	17	18
A_b (m^2)	9.9081	10.161	10.445	10.762	11.111	11.496	11.918	12.377	12.878
I_b (m^4)	16.215	17.238	18.41	19.745	21.257	22.964	24.885	27.043	29.462

embankment is equal to the other, i.e., $L_r = 30$ m); $E_r = 2.06 \times 10^{11}$ Pa; $I_r = 2 \times 2.037 \times 10^{-5}$ m^4; $m_r = 2 \times 51.5$ kg/m; $k_{rr} = k_{rb} = 2 \times 6.58 \times 10^7$ N/m^2; and $c_{rr} = c_{rb} = 2 \times 3.21 \times 10^4$ N·s/m^2.

According to an existing high-speed railway bridge in China, the following data are used for the bridge: $E_b = 3.55 \times 10^{10}$ Pa; $\rho_b = 2550$ kg/m^3; and $\zeta = 0.025$. A train consisting of five identical vehicles is considered, i.e., $N_v = 5$, and the Hertz spring stiffness $k_H = 2 \times 1.4 \times 10^9$ N/m[21].

The integral computational model is the same as the one shown in Fig.1. The dynamic responses of the vehicle-rail-bridge interaction with the four-span non-uniform continuous box girder bridge on a high-speed railway are studied in the rest of this section.

4.2.1. Influence of different element length combinations

Two types of mesh for the bridge are considered. The first type of mesh (Mesh 1) has 160 elements, each with a length of 1 m. In the second type of mesh (Mesh 2), the bridge is divided into 42 elements according to the segment lengths shown in Fig.11(a). The first ten frequencies of the bridge are listed in Table 3. The results of the two types of mesh show relatively good agreement, and a relatively fine mesh corresponds to the flexible dynamic characteristics of the bridge.

Table 3. **Natural frequencies of different types of mesh (Hz)**

Mode	1	2	3	4	5	6	7	8	9	10
Mesh 1	3.079	4.674	7.230	8.155	12.346	15.379	22.998	24.999	28.798	32.024
Mesh 2	3.092	4.696	7.274	8.186	12.431	15.455	23.167	25.106	28.947	32.220

In order to study the influence of different rail-bridge models on the dynamic response of the interaction system, three combination cases are examined:

Case I: Mesh 2 for the bridge and Mesh 1 for the rail lying on the bridge.

Case II: Mesh 1 for the bridge and the rail lying on the bridge.

Case III: Mesh 2 for the bridge and the rail lying on the bridge.

In these three cases, the rail lying on each embankment is divided into 30 equal elements, each with a length of 1 m. Obviously, Case II, in which the lengths of all elements are 1 m, has the finest meshes, and its results are supposed to be accurate. The dynamic responses of the bridge, rail and vehicle for different cases at various vehicle speeds ranging from 50 to 425 km/h are shown in Figs.12-16. Figures 12 and 13 show the maximum mid-span vertical displacement and acceleration of the bridge at the left central span, respectively. From Fig.12, it can be observed that the dynamic responses in the three cases are relatively consistent at the same speeds, although the results of Case II are slightly larger

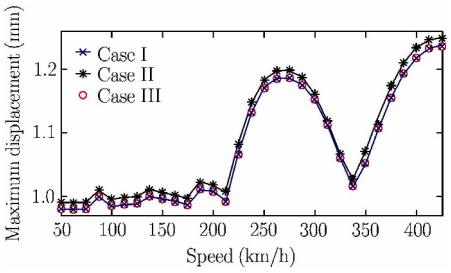

Fig. 12. Maximum mid-span vertical displacement of bridge.

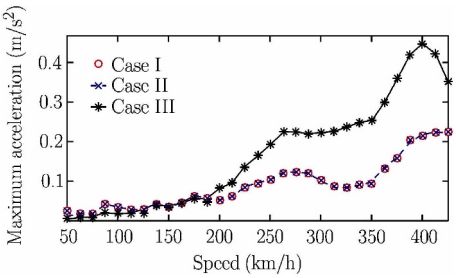

Fig. 13. Maximum mid-span vertical acceleration of bridge.

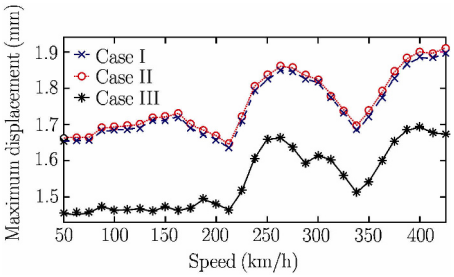

Fig. 14. Maximum vertical displacement of rail at the mid-span.

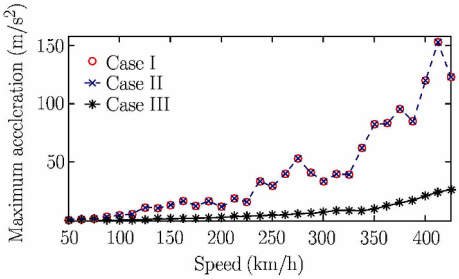

Fig. 15. Maximum vertical acceleration of rail at the mid-span.

than those of the other two. A possible reason for such small differences is the finer mesh for the bridge in Case II. From Fig.13, it can be seen that the dynamic responses in Case I and Case II show good agreement, but those in Case III are much different. These results indicate that the length of the rail element has an important influence on the dynamic response of the bridge, and that a rail element with a relatively small length can ensure more accurate results.

Figures 14 and 15 show the maximum vertical displacement and acceleration of the rail at the mid-span of the left central span, respectively. From Fig.14, it can be seen that Case I and Case II show good agreement, but the results for Case III have obvious differences compared with the other two cases. From Fig.15, it is clear that Case I and Case II also show good agreement with respect to vertical acceleration. However, the results of Case III vary insignificantly compared with the other two cases; the maximum vertical acceleration in Case I is significantly greater than that in Case III. These results indicate that the bridge element length has less influence on the dynamic response of the rail, but the rail element length has significant effects.

Figure 16 shows the maximum vertical acceleration at the centroid of the central car body. Excellent agreement between Case I and Case II can be observed, but there are clear differences between the results of Case I and Case III. The maximum acceleration in Case III is obviously greater than that in Case I (e.g., about 1.5 times greater at a speed of 350 km/h). This indicates that the vehicle response is also sensitive to the mesh length of the rail element.

Figure 17 shows the time history of the contact force between the front wheelset of the central car and the rail in Case I and Case II at a speed of 200 km/h. Excellent agreement can be observed between the two cases, indicating that a relatively large bridge element length in the coupling element can ensure accurate results when the length of the rail element is small enough; this can also save computational time. Figure 18 shows the time history of the contact force between the front wheelset of the central car and the rail in Case I and Case III at a speed of 200 km/h. There is obvious disagreement between the two cases, and this indicates that a relatively small and uniform rail element length in the coupling element is necessary to ensure accurate results.

In summary, compared with Case III, Case I and Case II demonstrate good accuracy. Compared with Case II, Case I can save time because of the drastic reduction in DOFs. Our computations show that the total CPU times in Case II and Case I are 225.9 s and 105.8 s, respectively, for a 3.0 GHz PC (the

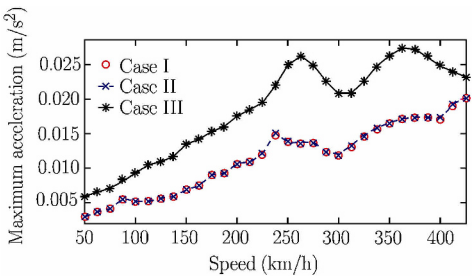

Fig. 16. Maximum vertical acceleration of central car body.

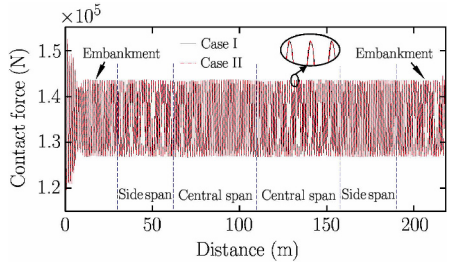

Fig. 17. Contact force of Case I and Case II at $v = 200$ km/h.

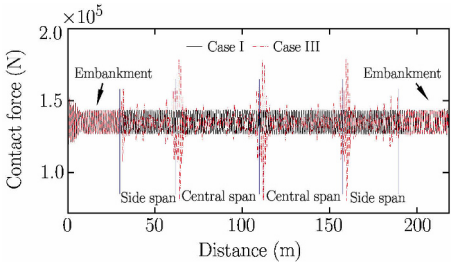

Fig. 18. Contact force of Case I and Case III at $v = 200$ km/h.

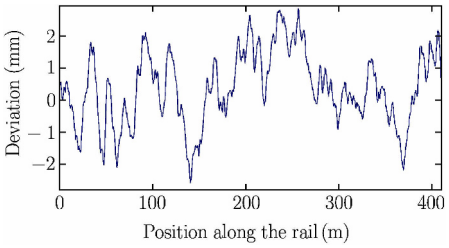

Fig. 19. Rail irregularity profile generated for FRA Class 6 track.

ratio of the latter to the former is about 0.47). In addition, 18 key sections should be calculated for Case II, but only 5 key sections should be calculated for Case I. Therefore, considering both accuracy and efficiency, it is suggested that a combination of a relatively large bridge element length and a relatively small rail element length should be adopted in the integrated coupling element, and the structure model of Case I will be utilized in the following study.

4.2.2. Influence of rail random irregularity

Rail irregularity represents an important excitation source for the train and the bridge, and it has an important influence on the system dynamic responses. Usually, the rail irregularity is assumed to be a random function characterized by the power spectral density (PSD) function as follows[1,30]:

$$S(\Omega) = \frac{A\Omega_2^2}{(\Omega^2 + \Omega_1^2)(\Omega^2 + \Omega_2^2)} \tag{34}$$

where Ω (rad/m) denotes the spatial frequency, and Ω_1, Ω_2 and A (m^3) are constants determined by the Federal Railroad Administration (FRA[1], in which Ω_1 and Ω_2 depend on the irregularity type and A depends on both the irregularity type and rail quality.

The FRA has classified rail quality into six classes (1-6), where Class 6 represents the best and Class 1 the worst. In this study, Class 6 track is adopted, and the generated irregularity profile is shown in Fig.19.

In order to demonstrate the function of the integrated coupling element, the dynamic responses based on the proposed wheel-rail contact model (Present model) are compared with those of the traditional wheel-rail interaction model (Traditional model), in which each wheelset is assumed to always maintain contact with the rail[12–14] and the primary suspensions between wheels and bogies are taken as the interaction interfaces[19].

Figures 20 and 21 show the maximum mid-span vertical displacement and acceleration of the bridge at the left central span, respectively. From Fig.20, it can be observed that the vertical displacement is consistent for different surfaces and models. This implies that the irregularity has less influence on the bridge displacement. From Fig.21, it can be seen that, when considering irregularity, the vertical acceleration of the bridge based on the present model is greater than that based on the traditional model, indicating the importance of considering the wheel-rail contact. The maximum vertical displacement of the rail at the mid-span of the left central span is shown in Fig.22. Regardless of the contact model,

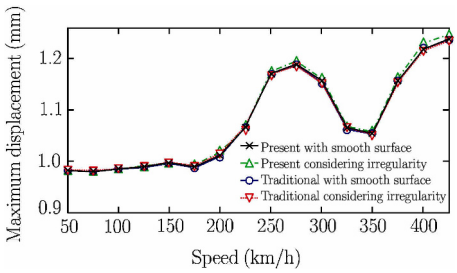

Fig. 20. Maximum mid-span vertical displacement of bridge.

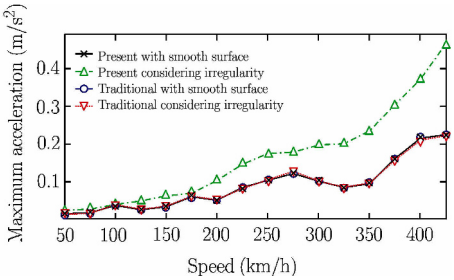

Fig. 21. Maximum mid-span vertical acceleration of bridge.

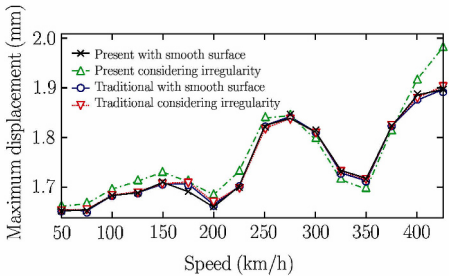

Fig. 22. Maximum vertical displacement of rail at the mid-span.

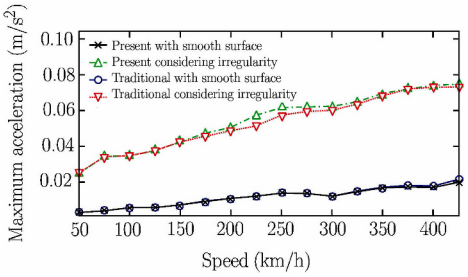

Fig. 23. Maximum vertical acceleration of central car body.

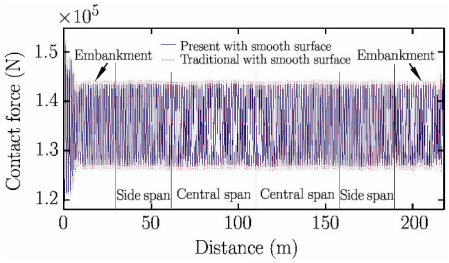

Fig. 24. Contact force of smooth surface.

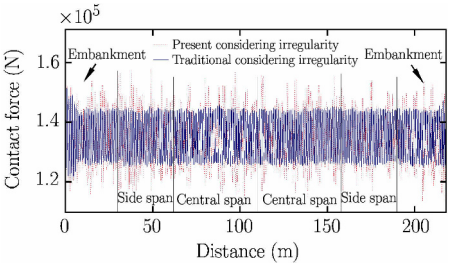

Fig. 25. Contact force considering random irregularity.

the influence of the irregularity on the rail displacement is limited. Besides, because of the elasticity of rail bed, the displacement of rail is larger than that of bridge at the same speeds.

Figure 23 shows the maximum vertical acceleration at the centroid of the central car body at different speeds. It is interesting that the two models agree very well for both smooth and irregular surfaces. So, if the vehicle response is of major concern, the effect of the wheel-rail interface may be ignored. Figure 24 shows the time history of the contact force on the smooth surface at a speed of 200 km/h. Excellent agreement can be observed between the two models. Figure 25 shows the time history of the contact force with random irregularity at a speed of 200 km/h. It can be seen that the contact force based on the present model is greater than that based on the traditional model. This may be because the stiffness of the Hertz spring is much greater than that of the primary suspension.

Comparing the two wheel-rail interaction models, one may find that the excitation induced by the irregularity in the vehicle-rail-bridge interaction system is realized by the Hertz spring in the present model, whereas by the primary suspension (i.e., k_1 and c_1) in the traditional model[19]. Therefore, the dynamic responses of the two models are consistent when the surface is smooth. However, when considering irregularity, the traditional model may underestimate the dynamic responses of the subsystems below the contact interface.

4.2.3. Influence of rail abrupt irregularity

In modern high-speed railway bridge construction, more and more long bridges suffer from rail joint and broken rail irregularity due to deformation; this will increase the dynamic responses of the bridge and the train, and therefore cannot be ignored in the design and maintenance of railway bridges. In this section, the dynamic responses of the bridge with rail abrupt irregularity under a moving train travelling at a speed of 360 km/h are examined. Another aim is to test and simulate a transient jump phenomenon using the present model.

Suppose that the abrupt irregularity is located on the central pier, which may be characterized by the following expression[1]:

$$r(x) = D\mathrm{e}^{-k|x|} \tag{35}$$

where $D = 6.4$ mm and $k = 0.46$ m^{-1}.

From Fig.26, it can be seen that the present model and the traditional model show good agreement in terms of bridge displacement. However, as shown in Fig.27, there are manifest differences between the two models with respect to bridge acceleration; the impact induced by the abrupt irregularity on bridge acceleration based on the present model is more significant than that based on the traditional

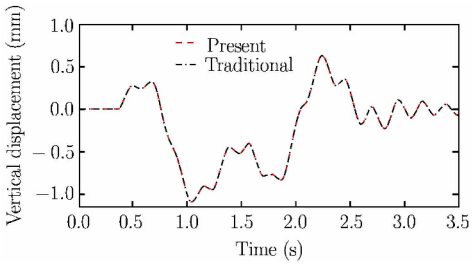

Fig. 26. Mid-span vertical displacement of bridge with abrupt irregularity.

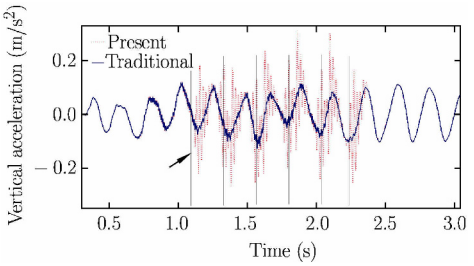

Fig. 27. Mid-span vertical acceleration of bridge with abrupt irregularity.

model. As shown in Fig.28, the rail accelerations show similar patterns of results. The vertical relative displacement of the rail to bridge at the mid-span is shown in Fig.29. The relative displacement is very small because of the strong constraint effect of the rail bed, and the periodic excitation formed by the series of axle loads causes periodic forced vibration of the rail. In addition, the results of the two models agree quite well with each other, implying the insignificant influence of the abrupt irregularity on the relative displacement.

Figure 30 shows the time history of the vertical acceleration at the centroid of the central car body. It can be seen that the maximum acceleration of car body based on the present model is larger than that of the traditional model in the time range of 1.55 s to 1.85 s. Also, because of the suspension system of the vehicle, the impact induced by the abrupt irregularity will be damped out after the vehicle exits from the central pier. Figure 31 shows the time history of the contact force between the front wheelset and the rail. It can be observed that the impact of abrupt irregularity on the contact force measured by the present model is more pronounced than that of the traditional model. The minimum contact force based on the present model decreases to zero at certain times, indicating transient jumps of the wheel. These results also indicate that transient jumps of the wheel can be simulated by the present model but not by the traditional model.

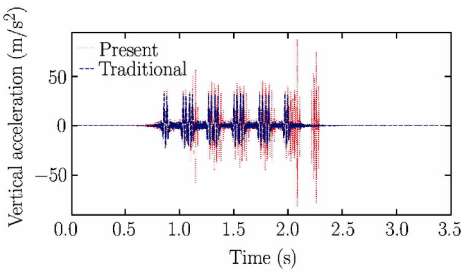

Fig. 28. Vertical acceleration of rail at the mid-span with abrupt irregularity.

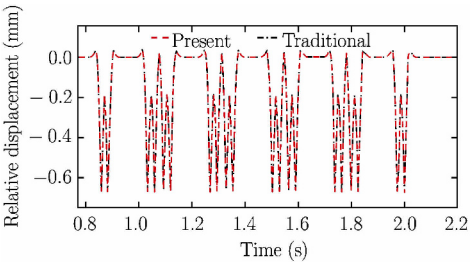

Fig. 29. Vertical relative displacement of the rail to bridge at the mid-span with abrupt irregularity.

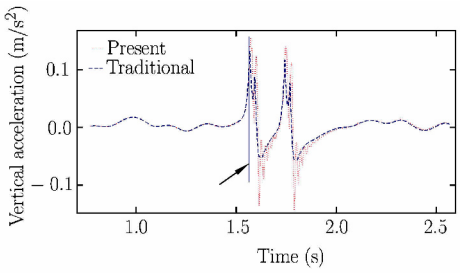

Fig. 30. Vertical acceleration of central car body with abrupt irregularity.

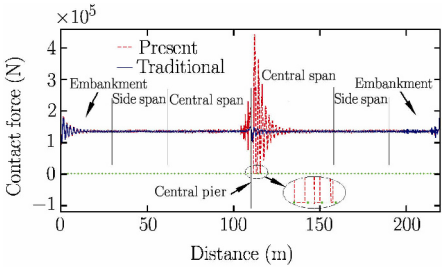

Fig. 31. Contact force considering abrupt irregularity.

V. CONCLUSIONS

An integrated vehicle-rail-bridge coupling element considering the wheel-rail interface is proposed for analyzing the dynamic response of a non-uniform continuous railway bridge travelled on by high-speed trains. The vehicle, the rail and the bridge are regarded as three interactive subsystems in the integrated coupling element and, based on the substructure principle[28], the equations of motion for the coupling element can be established. These equations are time-dependent and can be solved by the step-by-step integration method to simultaneously obtain the dynamic response of each subsystem. The accuracy, efficiency and function of the integrated coupling element are tested by two numerical examples, in which the influences of random and abrupt irregularities on the dynamic responses based on the present contact model are compared with those based on the traditional wheel-rail interaction model. From the numerical results, the following conclusions can be drawn:

(1) The simplified calculation method developed for the complex non-uniform beam is able to guarantee superior accuracy and efficiency, and the present wheel-rail contact model should be used when jumps of wheel are taken into consideration.

(2) The lengths of the rail element have a significant influence on the accuracy of the dynamic responses, especially the contact force, while the effect of the bridge element lengths is proved limited. Thus, in order to improve the efficiency of computation and modelling, a relatively large bridge element length (e.g., segment length) should be adopted in the coupling element for non-uniform continuous bridges.

(3) The random irregularity can have significant influences on the system dynamic responses, especially the car body acceleration, which is usually taken as the riding comfort index. The abrupt irregularity can appreciably increase the responses, and lead to jumps of wheel, jeopardizing the running safety of train. Therefore, maintaining a smooth rail surface in railway engineering is very important.

(4) With the irregularities neglected, the results of the present model are relatively consistent with those of the traditional model; however, in consideration of the irregularities, it is necessary to take into account the wheel-rail contact interface. Besides, the approach of the proposed coupling element can be easily extended to more complicated composite structures, such as cable-stayed bridges.

References

[1] Frýba,L., Dynamics of Railway Bridges. London: Thomas Telford House, 1996.

[2] Frýba,L., Vibration of Solids and Structures under Moving Loads. Czech Republic: Thomas Telford House, 1999.

[3] Yang,Y.B., Yau,J.D. and Wu,Y.S., Vehicle-Bridge Interaction Dynamics: With Applications to High-Speed Railways. Singapore: World Scientific Publishing, 2004.

[4] Yang,Y.B. and Yau,J.D., Vehicle-bridge interaction element for dynamic analysis. *Journal of Structural Engineering*, 1997, 123(11): 1512-1518.

[5] Yang,Y.B., Chang,C.H. and Yau,J.D., An element for analyzing vehicle-bridge systems considering vehicle's pitching effect. *International Journal for Numerical Methods in Engineering*, 1999, 46(7): 1031-1047.

[6] Wu,C., Liu,X.W. and Huang,X.C., Alterable-element method for vehicle-bridge interaction considering the transient jump of wheel. *Journal of Shanghai Jiaotong University (Science)*, 2008, 13: 330-335.

[7] Ju,S.H. and Lin,H.T., A finite element model of vehicle-bridge interaction considering braking and acceleration. *Journal of Sound and Vibration*, 2007, 303(1-2): 46-57.

[8] ERRI D214 Committee, Rail bridges for speeds higher than 200 km/h. Utrecht: Research report of the European Rail Research Institute, 1999.

[9] Cheng,Y.S., Au,F.T.K. and Cheung,Y.K., Vibration of railway bridges under a moving train by using bridge-track-vehicle element. *Engineering Structures*, 2001, 23: 1597-1606.

[10] Koh,C.G., Ong,J.S.Y., Chua,D.K.H. and Feng,J., Moving element method for train-track dynamics. *International Journal for Numerical Methods in Engineering*, 2003, 56: 1549-1567.

[11] Lou,P., A vehicle-track-bridge interaction element considering vehicle's pitching effect. *Finite Elements in Analysis and Design*, 2005, 41(4): 397-427.

[12] Lou,P. and Zeng,Q.Y., Formulation of equations of motion of finite element form for vehicle-track-bridge interaction system with two types of vehicle model. *International Journal for Numerical Methods in Engineering*, 2005, 62(3): 435-474.

[13] Lou,P., Finite element analysis for train-track-bridge interaction system. *Archive of Applied Mechanics*, 2007, 77(10): 707-728.

[14] Lou,P., Yu,Z.W. and Au,F.T.K., Rail-bridge coupling element of unequal lengths for analysing train-track-bridge interaction systems. *Applied Mathematical Modelling*, 2012, 36(4): 1395-1414.
[15] Yang,H.Y., Chen,Z.J., Zhang,H.L. and Huang,W., Vibration analysis of bridge under trains considering transient jump of wheel. *Journal of Chongqing Jiaotong University (Natural Science)*, 2014, 33(2): 21-25 (in Chinese).
[16] Yang,H.Y., Chen,Z.J., Zhang,H.L. and Fan,J.P., Dynamic analysis of train-rail-bridge interaction considering concrete creep of a multi-span simply supported bridge. *Advances in Structural Engineering*, 2014, 17(5): 709-720.
[17] Kargarnovin,M.H., Younesian,D., Thompson,D. and Jones,C., Ride comfort of high-speed trains travelling over railway bridges. *Vehicle System Dynamics*, 2005, 43(3): 173-199.
[18] Dinh,V.N., Kim,K.D. and Warnitchai,P., Simulation procedure for vehicle-substructure dynamic interactions and wheel movements using linearized wheel-rail interfaces. *Finite Elements in Analysis and Design*, 2009, 45(5): 341-356.
[19] Dinh,V.N., Kim,K.D. and Warnitchai,P., Dynamic analysis of three-dimensional bridge-high-speed train interactions using a wheel-rail contact model. *Engineering Structures*, 2009, 31(12): 3090-3106.
[20] Cheng,Y.S., Au,F.T.K., Cheung,Y.K. and Zheng,D.Y., On the separation between moving vehicles and bridge. *Journal of Sound and Vibration*, 1999, 222(5): 781-801.
[21] Bowe,C.J. and Mullarkey,T.P., Wheel-rail contact elements incorporating irregularities. *Advances in Engineering Software*, 2005, 36(11-12): 827-837.
[22] Zhang,Q.L., Vrouwenvelder,A. and Wardenier,J., Numerical simulation of train-bridge interactive dynamics. *Computers and Structures*, 2001, 79(10): 1059-1075.
[23] Liu,X.W., Xie,J., Wu,C. and Huang,X.C., Semi-analytical solution of vehicle-bridge interaction on transient jump of wheel. *Engineering Structures*, 2008, 30(9): 2401-2412.
[24] Leung,A.Y.T., Galerkin element method for non-uniform frames. *Computers and Structures*, 1995, 54(5): 819-834.
[25] Zheng,D.Y., Cheung,Y.K., Au,F.T.K. and Cheng,Y.S., Vibration of multi-span non-uniform beams under moving loads by using modified beam vibration functions. *Journal of Sound and Vibration*, 1998, 212(3): 455-467.
[26] Dugush,Y.A. and Eisenberger,M., Vibrations of non-uniform continuous beams under moving loads. *Journal of Sound and Vibration*, 2002, 254(5): 911-926.
[27] Martínez-Castro,A.E., Museros,P. and Castillo-Linares,A., Semi-analytic solution in the time domain for non-uniform multi-span Bernoulli-Euler beams traversed by moving loads. *Journal of Sound and Vibration*, 2006, 294(1-2): 278-297.
[28] Biondi,B., Muscolino,G. and Sofi,A., A substructure approach for the dynamic analysis of train-track-bridge system. *Computers and Structures*, 2005, 83(28-30): 2271-2281.
[29] Ates,S., Numerical modeling of continuous concrete box girder bridges considering construction stages. *Applied Mathematical Modelling*, 2011, 35: 3809-3820.
[30] Yau,J.D., Wu,Y.S. and Yang,Y.B., Impact response of bridges with elastic bearings to moving loads. *Journal of Sound and Vibration*, 2001, 248: 9-30.